An analytical and numerical study of peristaltic transport of a Johnson–Segalman fluid in an endoscope

Noreen Sher Akbar[a)†] and S. Nadeem[b)]

[a)] DBS&H, CEME, National University of Sciences and Technology, Islamabad, Pakistan
[b)] Department of Mathematics, Quaid-i-Azam University 45320, Islamabad 44000, Pakistan

(Received 31 May 2012)

In the present study, we discuss the peristaltic flow of a Johnson–Segalman fluid in an endoscope. Perturbation, homotopy, and numerical solutions are found for the non-linear differential equation. The comparative study is also made to check the validity of the solutions. The expressions for pressure rise frictional forces, pressure gradient, and stream lines are presented to interpret the behavior of various physical quantities of the Johnson–Segalman fluid.

Keywords: peristaltic pumping, Johnson–Segalman fluid, endoscope

PACS: 47.50.–d **DOI:** 10.1088/1674-1056/22/1/014703

1. Introduction

Peristaltic flows are important phenomena occurring in physiology and industry. Most situations like the transport of urine from the kidney to the bladder through the ureter, the movement of chyme in the gastrointestinal tract, the movement of spermatozoa in the ductus afferent of the male reproductive tract and the ovum in the female fallopian tube, the locomotion of some worms, the lymph transport in the lymphatic vessels and vasomotion of small blood vessels such as arterioles, venules, and capillaries, involve peristaltic motion. Further, peristaltic pumping occurs in many practical applications involving biomechanical systems, such as finger and roller pumps and heart lung machines.

A vast amount of studies are now found in the literature, which include analytical, numerical, and experimental studies[1–7] of peristaltic flows in different geometries. The study of non-Newtonian fluids is important due to their large number of applications. Non-Newtonian fluids are involved in food mixing, chyme movement in the intestine, plasma flow, blood flow, liquid flow, metal and alloy flows, mercury amalgam flow, and lubrication with heavy oils and greases. Most of the physiological fluids are non-Newtonian in nature. There are many non-Newtonian fluid models, some of them are tested experimentally, and some others are treated theoretically.[8–22]

The Johnson–Seagalman model is an integral model, which can also be written as a rate type model. The Johnson–Segalman model is a viscoelastic fluid model, which allows non-affine deformations.[23] Researchers[24–27] have used this model to explain the spurt phenomenon. Several experimentalists associated the spurt with a slip at a wall. Rao and Rajagopal[28] studied three distinct flows of the Johnson–Segalman type. The model was tested analytically by Ealshahed and Haroun.[29] They presented the peristaltic transport of Johnson–Segalman fluid under a magnetic field. Nadeem and Akbar[30] have discussed the peristaltic flow of a Johnson–Seagalman fluid in a non-uniform tube. The effect of magnetic field on the motion of a Johnson–Segalman fluid has been modeled by Hayat and Ali.[31]

Motivated by the above analysis, we discuss the peristaltic flow of a Johnson–Seagalman fluid in an endoscope. The governing equations are simplified by using long-wavelength and low-Reynold number approximations. The reduced problem is solved by using three methods, namely, (i) the perturbation method, (ii) the homotopy analysis method, and (iii) the shooting method. A comparison of analytical and numerical solutions is made, and an excellent agreement of all the solutions is found. The effects of different physical parameters appearing in the problem are discussed and shown graphically.

2. Mathematical model

Consider an incompressible fluid, for which the continuity and the momentum equations can be written as

$$\operatorname{div}\bar{\boldsymbol{V}} = 0, \tag{1}$$

$$\rho \frac{\mathrm{d}\bar{\boldsymbol{V}}}{\mathrm{d}t} = \operatorname{div}\boldsymbol{\sigma} + \rho \bar{\boldsymbol{f}}. \tag{2}$$

The Cauchy stress $\boldsymbol{\sigma}$ for a Johnson–Segalman fluid[29–31] is defined as

$$\boldsymbol{\sigma} = -P\boldsymbol{I} + \boldsymbol{T}, \tag{3}$$

where

$$\bar{\boldsymbol{T}} = 2\mu\bar{\boldsymbol{D}} + \bar{\boldsymbol{S}}, \tag{4}$$

$$\bar{\boldsymbol{S}} + m\Big(\frac{\mathrm{d}\bar{\boldsymbol{S}}}{\mathrm{d}t} + \bar{\boldsymbol{S}}(\bar{\boldsymbol{W}} - a\bar{\boldsymbol{D}}) + (\bar{\boldsymbol{W}} - a\bar{\boldsymbol{D}})^{\mathrm{T}}\bar{\boldsymbol{S}}\Big) = 2\eta\bar{\boldsymbol{D}}. \tag{5}$$

†Corresponding author. E-mail: noreensher@yahoo.com

© 2013 Chinese Physical Society and IOP Publishing Ltd

Here, $-P\boldsymbol{I}$ is the spherical part of the stress due to the constraint of incompressibility, $\bar{\boldsymbol{V}}$ is the velocity, $\bar{\boldsymbol{f}}$ is the body force, μ and η are the viscosities, m is the relaxation time, and a is the slip parameter. The $\bar{\boldsymbol{D}}$ and $\bar{\boldsymbol{W}}$ are the symmetric and the skewsymmetric parts of the velocity gradient respectively and can be defined as

$$\bar{\boldsymbol{D}} = \frac{1}{2}(\bar{\boldsymbol{L}} + \bar{\boldsymbol{L}}^{\mathrm{T}}), \tag{6a}$$

$$\bar{\boldsymbol{W}} = \frac{1}{2}(\bar{\boldsymbol{L}} - \bar{\boldsymbol{L}}^{\mathrm{T}}), \tag{6b}$$

where $\bar{\boldsymbol{L}} = \mathrm{grad}\bar{\boldsymbol{V}}$.

3. Problem formulation

We consider an incompressible Johnson–Segalman fluid in an endoscope. The flow is produced due to sinusoidal wave trains propagating with constant speed c along the walls of the endoscope. The geometry of the wall surface is defined as

$$\bar{R}_1 = a_1, \tag{7a}$$

$$\bar{R}_2 = a_2 + b\sin\frac{2\pi}{\lambda}(\bar{Z} - c\bar{t}), \tag{7b}$$

where $\bar{R}_1$ and $\bar{R}_2$ are the heights of the inner and the outer tubes, respectively, $\bar{Z}$ is the transverse component of the system, a_1 is the radius of the inner tube, a_2 is the radius of the outer tube at the inlet, b is the wave amplitude, λ is the wavelength, c the wave speed, and $\bar{t}$ is the time. The geometry is shown in Fig. 1.

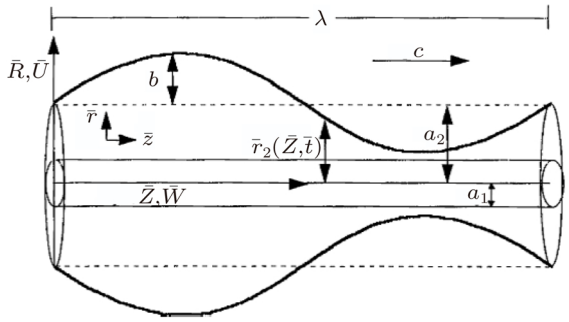


Fig. 1. Geometry of the problem.

The governing equations in the fixed frame for an incompressible flow are given as

$$\frac{\partial\bar{U}}{\partial\bar{R}} + \frac{\bar{U}}{\bar{R}} + \frac{\partial\bar{W}}{\partial\bar{Z}} = 0, \tag{8}$$

$$\rho\Big(\frac{\partial}{\partial\bar{t}} + \bar{U}\frac{\partial}{\partial\bar{R}} + \bar{W}\frac{\partial}{\partial\bar{Z}}\Big)\bar{U} = -\frac{\partial\bar{P}}{\partial\bar{R}} + \frac{1}{\bar{R}}\frac{\partial}{\partial\bar{R}}(\bar{R}\bar{S}_{\bar{R}\bar{R}}) + \frac{\partial}{\partial\bar{Z}}(\bar{S}_{\bar{R}\bar{Z}}) + \Big(\frac{1}{\bar{R}}\frac{\partial}{\partial\bar{R}}\Big(\bar{R}\frac{\partial\bar{U}}{\partial\bar{R}}\Big) + \frac{\partial^2\bar{U}}{\partial\bar{Z}^2}\Big), \tag{9}$$

$$\rho\Big(\frac{\partial}{\partial\bar{t}} + \bar{U}\frac{\partial}{\partial\bar{R}} + \bar{W}\frac{\partial}{\partial\bar{Z}}\Big)\bar{W} = -\frac{\partial\bar{P}}{\partial\bar{Z}} + \frac{1}{\bar{R}}\frac{\partial}{\partial\bar{R}}(\bar{R}\bar{S}_{\bar{R}\bar{Z}}) + \frac{\partial}{\partial\bar{Z}}(\bar{S}_{\bar{Z}\bar{Z}}) + \Big(\frac{1}{\bar{R}}\frac{\partial}{\partial\bar{R}}\Big(\bar{R}\frac{\partial\bar{W}}{\partial\bar{R}}\Big) + \frac{\partial^2\bar{W}}{\partial\bar{Z}^2}\Big), \tag{10}$$

$$2\eta\frac{\partial\bar{U}}{\partial\bar{R}} = \bar{S}_{\bar{R}\bar{R}} + m\Big(\frac{\partial}{\partial\bar{t}} + \bar{U}\frac{\partial}{\partial\bar{R}} + \bar{W}\frac{\partial}{\partial\bar{Z}}\Big)\bar{S}_{\bar{R}\bar{R}} - 2am\bar{S}_{\bar{R}\bar{R}}\frac{\partial\bar{U}}{\partial\bar{R}} + m\Big((1-a)\frac{\partial\bar{W}}{\partial\bar{R}} - (1+a)\frac{\partial\bar{U}}{\partial\bar{Z}}\Big)\bar{S}_{\bar{R}\bar{Z}}, \tag{11}$$

$$\eta\Big(\frac{\partial\bar{U}}{\partial\bar{Z}} + \frac{\partial\bar{W}}{\partial\bar{R}}\Big) = \bar{S}_{\bar{R}\bar{Z}} + m\Big(\frac{\partial}{\partial\bar{t}} + \bar{U}\frac{\partial}{\partial\bar{R}} + \bar{W}\frac{\partial}{\partial\bar{Z}}\Big)\bar{S}_{\bar{R}\bar{Z}} + \frac{m}{2}\Big((1-a)\frac{\partial\bar{U}}{\partial\bar{Z}} - (1+a)\frac{\partial\bar{W}}{\partial\bar{R}}\Big)\bar{S}_{\bar{R}\bar{R}} + \frac{m}{2}\Big((1-a)\frac{\partial\bar{W}}{\partial\bar{R}} - (1+a)\frac{\partial\bar{U}}{\partial\bar{Z}}\Big)\bar{S}_{\bar{Z}\bar{Z}}, \tag{12}$$

$$2\eta\frac{\partial\bar{W}}{\partial\bar{Z}} = \bar{S}_{\bar{Z}\bar{Z}} + m\Big(\frac{\partial}{\partial\bar{t}} + \bar{U}\frac{\partial}{\partial\bar{R}} + \bar{W}\frac{\partial}{\partial\bar{Z}}\Big)\bar{S}_{\bar{Z}\bar{Z}} - 2am\bar{S}_{\bar{Z}\bar{Z}}\frac{\partial\bar{W}}{\partial\bar{Z}} + m\Big((1-a)\frac{\partial\bar{U}}{\partial\bar{Z}} - (1+a)\frac{\partial\bar{W}}{\partial\bar{R}}\Big)\bar{S}_{\bar{R}\bar{Z}}, \tag{13}$$

where $\bar{S}_{\bar{R}\bar{R}}$, $\bar{S}_{\bar{Z}\bar{Z}}$, $\bar{S}_{\bar{R}\bar{Z}}$ are the components of the stress tensor in the radial and the transversal directions, $\bar{p}$ is the pressure, and $\bar{U}$ and $\bar{W}$ are the velocity components in the radial and the axial directions in the fixed frame, respectively.

Using the transformation

$$\bar{x} = \bar{X} - c\bar{t},\ \bar{y} = \bar{Y},$$
$$\bar{u} = \bar{U} - c,\ v = \bar{V}, \tag{14}$$

and dimensionless variables

$$R = \frac{\bar{R}}{a_1},\ r = \frac{\bar{r}}{a_1},\ Z = \frac{\bar{Z}}{\lambda},\ z = \frac{\bar{z}}{\lambda},\ W = \frac{\bar{W}}{c},$$
$$w = \frac{\bar{w}}{c},\ U = \frac{\lambda\bar{U}}{a_1 c},\ u = \frac{\lambda\bar{u}}{a_1 c},\ P = \frac{a_1^2\bar{P}}{c\lambda(\mu+\eta)},$$
$$t = \frac{c\bar{t}}{\lambda},\ \delta = \frac{a_1}{\lambda},\ We = \frac{mc}{a_1},\ Re = \frac{\rho c a_1}{\mu},\ \boldsymbol{S} = \frac{a_1\bar{\boldsymbol{S}}}{c\mu},$$
$$r_1 = \frac{\bar{r}_1}{a_1} = \varepsilon,\ r_2 = \frac{\bar{r}_2}{a_1} = 1 + \phi\sin(2\pi z), \tag{15}$$

where δ is the longwave length, and We is the Weissenberg number, we give Eqs. (8)–(13) at the lowest order of δ as

$$\Big(\frac{\mu+\eta}{\mu}\Big)\frac{\partial P}{\partial z} = \frac{\partial S_{rz}}{\partial r} + \frac{1}{r}\frac{\partial}{\partial r}\Big(r\frac{\partial w}{\partial r}\Big), \tag{16}$$

$$\frac{\partial P}{\partial r} = 0, \tag{17}$$

$$S_{rr} - We(1+a)\frac{\partial w}{\partial r}S_{rz}, \tag{18}$$

$$\frac{\eta}{\mu}\frac{\partial w}{\partial r} = S_{rz} + \frac{We}{2}(1-a)\frac{\partial w}{\partial r}S_{rr} - \frac{We}{2}(1+a)\frac{\partial w}{\partial r}S_{zz}, \tag{19}$$

$$S_{zz} - We(1+a)\frac{\partial w}{\partial r}S_{rz}. \tag{20}$$

Solving Eqs. (18)–(20), we get

$$S_{rr} = We(1+a)\frac{\eta}{\mu}\Big(\frac{\partial w}{\partial r}\Big)^2, \tag{21}$$

$$S_{zz} = -We(1-a)\frac{\eta}{\mu}\Big(\frac{\partial w}{\partial r}\Big)^2, \tag{22}$$

$$S_{rz} = \frac{\frac{\eta}{\mu}\frac{\partial w}{\partial r}}{1+We^2(1-a^2)\left(\frac{\partial w}{\partial r}\right)^2}. \tag{23}$$

With the help of Eqs. (21)–(23), we can write Eqs. (16) and (17) as

$$\frac{1}{r}\frac{\partial}{\partial r}\left[r\left(\frac{\frac{\eta}{\mu}\frac{\partial w}{\partial r}}{1+We^2(1-a^2)(\frac{\partial w}{\partial r})^2}\right)\right]+\frac{1}{r}\frac{\partial}{\partial r}\left(r\frac{\partial w}{\partial r}\right) = \left(\frac{\mu+\eta}{\mu}\right)\frac{\partial P}{\partial z}, \tag{24}$$

$$\frac{\mathrm{d}P}{\mathrm{d}r} = 0. \tag{25}$$

The corresponding boundary conditions for the problem are

$$w = -1, \text{ at } r = r_1 = \varepsilon, \tag{25a}$$

$$w = -1, \text{ at } r = r_2 = 1+\phi\sin(2\pi z). \tag{25b}$$

4. Perturbation solution

Equation (24) is a highly non-linear differential equation, and we are interested in calculating its analytical solution. Therefore we use the regular perturbation method. For the perturbation solution, we express w, $(\mathrm{d}P)/(\mathrm{d}z)$, and Q (flow rate) as[24]

$$w = w_0 + We^2 w_1 + \mathrm{O}(We^4), \tag{26a}$$

$$\frac{\mathrm{d}p}{\mathrm{d}z} = \frac{\mathrm{d}p_0}{\mathrm{d}z} + We^2\frac{\mathrm{d}p_1}{\mathrm{d}z} + \mathrm{O}(We^4), \tag{26b}$$

$$Q = Q_0 + We^2 Q_1 + \mathrm{O}(We^4). \tag{26c}$$

Invoking Eqs. (26a)–(26c) in Eqs. (24) and (25), and comparing the like power of We^2, we have the following systems.

4.1. Zeroth-order system

$$\frac{\mathrm{d}p_0}{\mathrm{d}r} = 0, \tag{27}$$

$$\left(\frac{\mu+\eta}{\mu}\right)\frac{\partial P_0}{\partial z} = \frac{1}{r}\frac{\partial}{\partial r}\left(\frac{\eta}{\mu}r\frac{\partial w_0}{\partial r}\right)+\frac{1}{r}\frac{\partial}{\partial r}\left(r\frac{\partial w_0}{\partial r}\right), \tag{28}$$

$$w_0 = -1, \text{ at } r = r_1 = \varepsilon, \tag{28a}$$

$$w_0 = -1, \text{ at } r = r_2 = 1+\phi\sin(2\pi z). \tag{28b}$$

4.2. First-order system

$$\frac{\mathrm{d}p_1}{\mathrm{d}r} = 0, \tag{29}$$

$$\left(\frac{\mu+\eta}{\mu}\right)\frac{\partial P_1}{\partial z} = \frac{1}{r}\frac{\partial}{\partial r}\left(\frac{\eta}{\mu}r\frac{\partial w_1}{\partial r}\right) + \left(a^2-1\right)\frac{1}{r}\frac{\partial}{\partial r}\left(\frac{\eta}{\mu}r\left(\frac{\partial w_0}{\partial r}\right)^3\right) + \frac{1}{r}\frac{\partial}{\partial r}\left(r\frac{\partial w_1}{\partial r}\right), \tag{30}$$

$$w_1 = 0, \text{ at } r = r_1 = \varepsilon, \tag{30a}$$

$$w_1 = 0, \text{ at } r = r_2 = 1+\phi\sin(2\pi z). \tag{30b}$$

4.3. Solution of the zeroth-order system

The solutions of Eq. (28) satisfying Eqs. (28a) and (28b) are

$$w_0 = -1+\left(\frac{r^2}{4}+A_1\ln r+A_2\right)\frac{\partial P_0}{\partial z}, \tag{31}$$

$$\frac{\mathrm{d}p_0}{\mathrm{d}z} = \frac{2F_0+(r_2^2-r_1^2)}{A_5}. \tag{32}$$

4.4. Solution of the first-order system

Invoking the value of w_0 in Eq. (30), we can write the solution satisfying conditions (30a) and (30b) as

$$w_1 = \left(\frac{r^2}{4}+A_1\ln r+A_2\right)\frac{\partial P_1}{\partial z}+(1-a^2)\frac{\eta}{\mu+\eta}\left(\frac{\partial P_0}{\partial z}\right)^3\left(\frac{r^4}{32}-\frac{2A_1}{r^2}+\frac{3A_1r^2}{8}+\frac{3A_1^2}{2}\ln r\right)+A_3\ln r+A_4, \tag{33}$$

$$\frac{\mathrm{d}p_1}{\mathrm{d}z} = \frac{2F_1-A_6}{A_5}. \tag{34}$$

Summarizing the perturbation results for small parameter We^2, we can write the expressions for velocity field and pressure gradient as

$$w = -1+\left(\frac{r^2}{4}+A_1\ln r+A_2\right)\frac{\partial P}{\partial z}+We^2\left((1-a^2)\frac{\eta}{\mu+\eta}\left(\frac{\partial P_0}{\partial z}\right)^3\left(\frac{r^4}{32}-\frac{2A_1}{r^2}+\frac{3A_1r^2}{8}+\frac{3A_1^2}{2}\ln r\right)+A_3\ln r+A_4\right), \tag{35}$$

$$\frac{\mathrm{d}p}{\mathrm{d}z} = \frac{2F+(r_2^2-r_1^2)}{A_5}+We^2\left(-\frac{A_6}{A_5}\right), \tag{36}$$

where

$$A_1 = -\frac{(r_1^2-r_2^2)}{4(\ln r_1-\ln r_2)},\ A_2 = -\left(\frac{r_1^2}{4}+A_1\ln r_1\right),$$

$$A_3 = -\frac{(1-a^2)}{(\ln r_1-\ln r_2)}\frac{\eta}{\mu+\eta}\left(\frac{\partial P_0}{\partial z}\right)^3\left(\frac{r_1^4-r_2^4}{32}-\frac{2A_1}{r_1^2-r_2^2}+\frac{3A_1(r_1^2-r_2^2)}{8}+\frac{3A_1^2}{2}(\ln r_1-\ln r_2)\right),$$

$$A_4 = -\frac{(1-a^2)}{(\ln r_1 - \ln r_2)}\frac{\eta}{\mu+\eta}\left(\frac{\partial P_0}{\partial z}\right)^3\left(\frac{r_1^4}{32} - \frac{2A_1}{r_1^2} + \frac{3A_1 r_1^2}{8} + \frac{3A_1^2}{2}\ln r_1\right),$$

$$A_5 = \left(\frac{r_2^4 - r_1^4}{8} + A_1(r_2^2 \ln r_2 - r_1^2 \ln r_1) - \frac{A_1}{2}(r_2^2 - r_1^2) + A_2(r_2^2 - r_1^2)\right),$$

$$A_6 = -(1-a^2)\frac{\eta}{\mu+\eta}\left(\frac{\partial P_0}{\partial z}\right)^3\left(\frac{r_2^6 - r_1^6}{5} - 4A_1(\ln r_2 - \ln r_1) + \frac{3A_1(r_2^4 - r_1^4)}{4}\right.$$
$$\left. + 3A_1^2\left(\frac{r_2^2 \ln r_2 - r_1^2 \ln r_1}{2} - \frac{(r_2^2 - r_1^2)}{4}\right)\right) + A_3\left(r_2^2 \ln r_2 - r_1^2 \ln r_1 - \frac{(r_2^2 - r_1^2)}{2}\right) + A_4(r_2^2 - r_1^2).$$

The instantaneous volume flow rate in the fixed coordinate system is given by

$$Q = F + \frac{1}{2}\left(1 - \varepsilon^2 + \frac{\phi^2}{2}\right). \tag{36a}$$

The pressure rise ΔP and the friction forces on the inner and the outer tubes $F^{(0)}$, $F^{(\mathrm{i})}$ are calculated as

$$\Delta P = \int_0^1 \frac{\mathrm{d}p}{\mathrm{d}z}\mathrm{d}z, \tag{37}$$

$$F^{(0)} = \int_0^1 r_1^2\left(-\frac{\mathrm{d}p}{\mathrm{d}z}\right)\mathrm{d}z, \tag{38}$$

$$F^{(\mathrm{i})} = \int_0^1 r_2^2\left(-\frac{\mathrm{d}p}{\mathrm{d}z}\right)\mathrm{d}z, \tag{39}$$

where $\mathrm{d}p/\mathrm{d}z$ is defined in Eq. (36).

4.5. Homotopy analysis method solution

In this section, we use the homotopy analysis method (HAM) to find the solution of Eqs. (24) and (25). We choose

$$w_0 = -1 + \left(\frac{r^2}{4} + A_1 \ln r + A_2\right)\frac{\partial P}{\partial z} \tag{40}$$

as the initial guess. Furthermore, the auxiliary linear operator for the problem is taken as

$$\mathscr{L}_{wr}(w) = \frac{1}{r}\frac{\partial}{\partial r}\left(r\frac{\partial w_0}{\partial r}\right), \tag{41}$$

which satisfies

$$\mathscr{L}_{wr}(w_0) = 0. \tag{42}$$

From Eqs. (16) and (17), we can define the following zeroth-order deformation problem:

$$(1-q)\mathscr{L}_{wr}[\,\bar{w}(r,q) - w_0(r)] = q\hbar_w N_{wr}[\bar{w}(r,q)], \tag{43}$$

$$\bar{w}(r,q) = 0, \text{ at } r = r_1,$$

$$\bar{w}(r,q) = 0, \text{ at } r = r_2, \tag{44}$$

where $\hbar_w$ denotes the non-zero auxiliary parameter, $q \in (0,1]$ is the embedding parameter, and

$$N_{wr}[\bar{w}(r,q)] = \frac{\partial^2 w}{\partial r^2} + \frac{1}{r}\frac{\partial w}{\partial r} + \frac{a_{11}}{r}\left(\frac{\partial w}{\partial r}\right)^3 + 3a_{11}\frac{\partial^2 w}{\partial r^2}\left(\frac{\partial w}{\partial r}\right)^2 - \frac{\mathrm{d}p}{\mathrm{d}z}. \tag{45}$$

Obviously,

$$\hat{w}(r,0) = w_0,\ \hat{w}(r,1) = w(r), \tag{46}$$

when q varies from 0 to 1, $\hat{w}(r,q)$ varies from the initial guess to the solution $w(r)$. Expanding $\hat{w}(r,q)$ in Taylor's series with respect to the embedding parameter q, we have

$$\hat{w}(r,q) = w_0(r) + \sum_{n=1}^{\infty} w_m(r) q^m, \tag{47}$$

$$w_m = \frac{1}{m!}\frac{\partial^m \bar{w}(r,q)}{\partial q^m}\Big|_{q=0}. \tag{48}$$

Differentiating the zeroth-order deformation m times with respect to q, then dividing by $m!$, and finally setting $q = 0$, we get the following m-th-order deformation problem:

$$\mathscr{L}_w[w_m(r) - \chi_m w_{m-1}(r)] = \hbar_w R_{wr}(r), \tag{49}$$

where

$$R_{wr} = w''_{m-1} + \frac{1}{r}w'_{m-1} + \frac{a_{11}}{r}\sum_{i=0}^{m-1} w'_{m-1} w'_{m-1-i} w'_{m-k-1} + 3a_{11}\sum_{i=0}^{m-1} w'_{m-1} w'_{m-1-i} w''_{m-k-1} - \frac{\mathrm{d}p}{\mathrm{d}z}(1-\chi_m), \tag{50}$$

$$\chi_m = \begin{cases} 0, & m \le 1, \\ 1, & m > 1. \end{cases} \tag{51}$$

The solution of the above equation can be calculated with the help of Mathematica and is presented as follows:

$$w_m(r) = \lim_{M\to\infty}\left[\sum_{m=0}^{M} a_{m,0}^0 + \sum_{n=1}^{2M+1}\left(\sum_{m=n-1}^{2M}\sum_{k=1}^{2m+1-n} a_{m,n}^k r^n \ln r\right)\right] + \lim_{M\to\infty}\left[\sum_{n=1}^{2M+1}\left(\sum_{m=n-1}^{2M}\sum_{k=0}^{2m+1-n} a_{m,n}^k r^{2n+2}\right)\right], \tag{52}$$

where $a_{m,0}^0$ and $a_{m,n}^k$ are constants.

5. Numerical solution

The present problem consisting of Eqs. (24) can be also solved numerically by employing the shooting method. Because the analysis of the shooting method is found in many text books, the detail is not given here. The solution in term of graphs and tables are presented. The numerical results are also compared with the perturbation and HAM the results, see Figs. 3 and 4. Tables 1 and 2 present the comparison of per-

turbation, numerical, and HAM solutions.

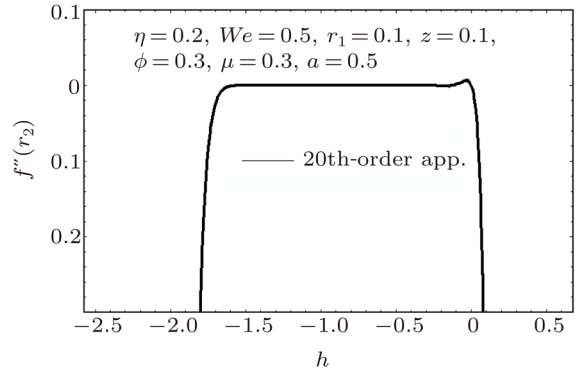


Fig. 2. The h-curve for velocity profile.

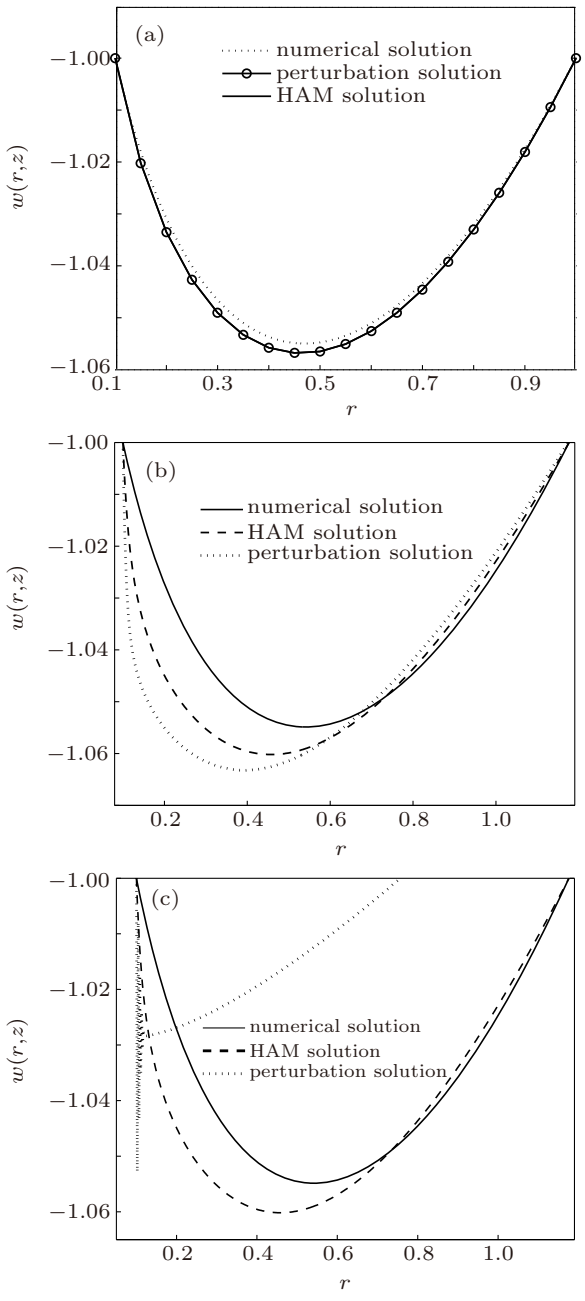


Fig. 3. Comparison of velocity profile for (a) $We = 0.5$, (b) $We = 0.8$, and (c) $We = 2$. The other parameters are $\eta = 0.2$, $\mu = 0.3$, $\varepsilon = 0.1$, $\phi = 0.3$, $a = 0.5$, and $z = 0.2$.

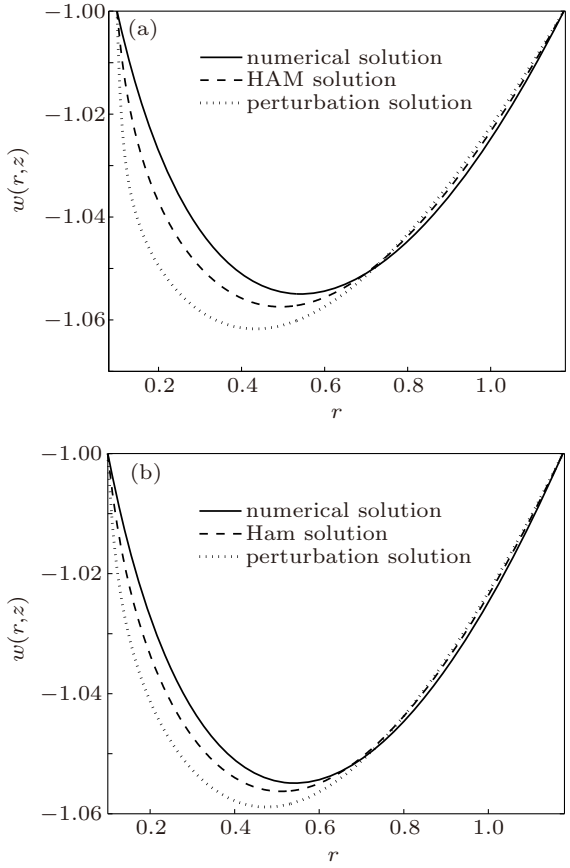


Fig. 4. Comparison of velocity profile for (a) $a = 100$ and (b) $a = 1000$. The other parameters are $\eta = 0.2$, $\mu = 0.3$, $We = 0.5$, $\varepsilon = 0.1$, $\phi = 0.3$, and $z = 0.2$.

Table 1. Comparison of the results for $\mu = 0.3$, $\varepsilon = 0.1$, $\phi = 0.3$, $a = 0.5$, $z = 0.2$, and $We = 0.5$.

r	Numerical	Perturbation	Error	HAM	Error
0.1	−1.00000	−1.00000	0.00000	−1.00000	0.00000
0.2	−1.03064	−1.03352	0.00270	−1.03350	0.00276
0.3	−1.04635	−1.04906	0.00258	−1.04904	0.00256
0.4	−1.05354	−1.05577	0.00211	−1.05576	0.00210
0.5	−1.05478	−1.05651	0.00163	−1.05650	0.00162
0.6	−1.05081	−1.05255	0.00165	−1.05255	0.00165
0.7	−1.04305	−1.04459	0.00147	−1.04458	0.00001
0.8	−1.03181	−1.03301	0.00116	−1.03301	0.00116
0.9	−1.01738	−1.01809	0.00069	−1.01809	0.00069
1.0	−1.00000	−1.00000	0.00000	−1.00000	0.00000

Table 2. Comparison of the present investigation with existing literatures for $\eta = 0.2$, $\mu = 0.3$, $\varepsilon = 0.1$, $\phi = 0.3$, $a = 0.5$, and $z = 0.2$.

r	Present work for $We = 0$	Ref. [4] for $\beta = 0$	Ref. [10] for $b^* = 0$	Ref. [18] for $1/\alpha = 0$
0.1	−1.00000	−1.00000	−1.00000	−1.00000
0.2	−1.02064	−1.02352	−1.02342	−1.03250
0.3	−1.03635	−1.03906	−1.03916	−1.04504
0.4	−1.04354	−1.04577	−1.04567	−1.05676
0.5	−1.04478	−1.04651	−1.04641	−1.05750
0.6	−1.04081	−1.04255	−1.04245	−1.05155
0.7	−1.03305	−1.03459	−1.03449	−1.04258
0.8	−1.04181	−1.04301	−1.04311	−1.03201
0.9	−1.00738	−1.00809	−1.00819	−1.01807
1.0	−1.00000	−1.00000	−1.00000	−1.00000

6. Discussion

In this section, the velocity, pressure rise, frictional forces, and axial pressure gradient are analyzed carefully. For this object, figures 3–24 are displayed. Figures 3(a) and 3(b) show that for small perturbation parameter, We, we have a good agreement between all the three results. Because the nonlinearity depends on We, when We is small, then we have weak nonlinearity. But for large We, the solutions deviate from each other, i.e., the error increases. Since We is taken as the perturbation parameter, its values cannot be greater than 1 in the perturbation method, but HAM and numerical solutions are valid and give convergent solutions when $We > 1$. Figures 4(a) and 4(a) show that for large values of a, the numerical, perturbation and the HAM solutions are valid. The pressure rise is calculated numerically by using Mathematica. Figures 3–5 show the pressure rise ΔP against volume flow rate Q for different values of Weisenberg number We, amplitude ratio ϕ, and radius ratio ε. These figures indicate that the pressure rise and the volume flow rate are inversely proportional to each other. As expected, the pressure rise obtains larger values for small volume flow rates and smaller values for large Q. Moreover, peristaltic pumping occurs in the region $-3 \leq Q \leq 1$ in Fig. 3, $-3 \leq Q \leq 0.5$ in Figs. 6 and 7, otherwise augmented pumping occurs. The pressure rise decreases with the increases of Weisenberg number We, amplitude ratio ϕ, and radius ratio ε. Figures 8–13 describe the variations of frictional forces. These figures show that the frictional forces have quite opposite features when compared with the pressure rise. So the frictional forces increase with the increases of Weisenberg number We, amplitude ratio ϕ, and radius ratio ε. The variations of pressure gradient are plotted in Figs. 14–20. The figures elucidate that the pressure gradient is large when $z \in [0, 0.5]$ and $z \in [1, 1.5]$ and small when $z \in [0.51, 1.49]$. Moreover, the pressure gradient decreases with the increasing We and μ while increases with the increases of η, a, ϕ, ε, and Q. It is also seen that the maximum pressure occurs at the center of the endoscope.

Another interesting phenomenon in peristaltic motion is trapping. It is basically the formation of an internally circulating bolus of fluid by the closed streamlines. This trapped bolus pushes ahead along with the peristaltic wave. Figures 21–24 show the trapping phenomenon for Q, μ, ϕ, and We. Figure 21 illustrates the streamlines for different values of time mean flow rate Q. It is observed that when we increase Q, the size of the trapped bolus increases. Figure 22 shows the streamlines for μ. It is shown that with the increase of μ, the number of trapping bolus decreases, but the size of the trapping bolus increases. Figures 23 and 24 are plotted to show the effects of ϕ and We, it is seen that the number of trapping bolus increases and the size of the trapping bolus decreases with the increase of ϕ, and the size of trapping bolus increases with the increase of We.

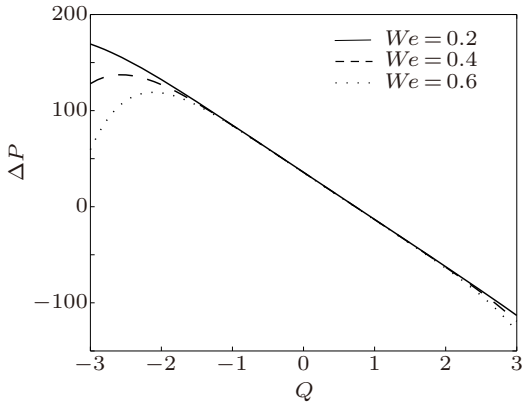


Fig. 5. Pressure rise versus flow rate for $\eta = 0.1$, $\mu = 0.2$, $\varepsilon = 0.5$, $\phi = 0.8$, and $a = 0.6$.

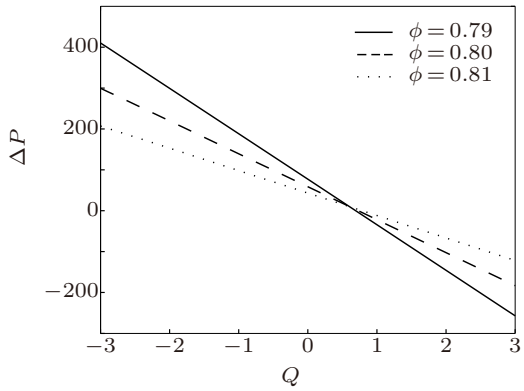


Fig. 6. Pressure rise versus flow rate for $\eta = 0.1$, $\mu = 0.1$, $\varepsilon = 0.3$, $We = 0.51$, and $a = 0.7$.

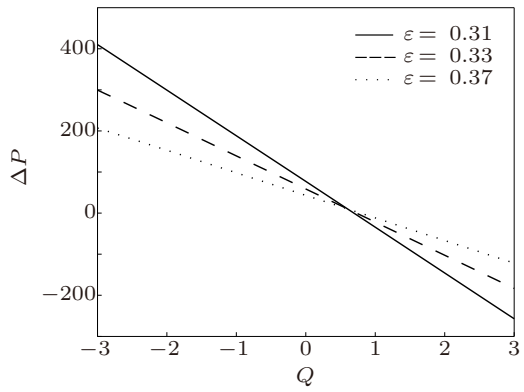


Fig. 7. Pressure rise versus flow rate for $\eta = 0.1$, $\mu = 0.1$, $\phi = 0.8$, $We = 0.6$, and $a = 0.8$.

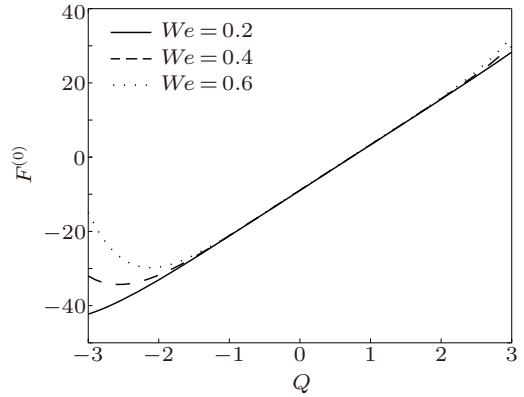


Fig. 8. Frictional force on the inner tube versus flow rate for $\eta = 0.1$, $\mu = 0.2$, $\varepsilon = 0.5$, $\phi = 0.8$, and $a = 0.6$.

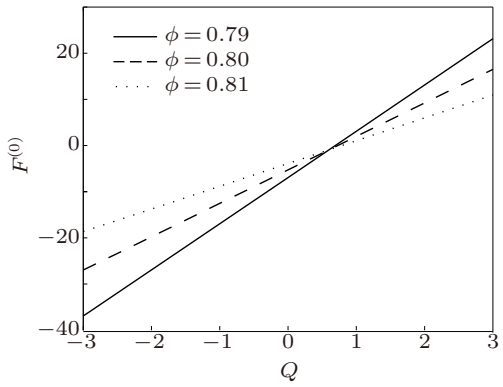


Fig. 9. Frictional force on the inner tube versus flow rate for $\eta = 0.1$, $\mu = 0.1$, $\varepsilon = 0.3$, $We = 0.51$, and $a = 0.7$.

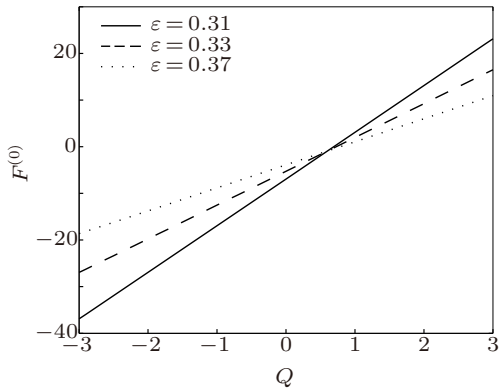


Fig. 10. Frictional force on the inner tube versus flow rate for $\eta = 0.1$, $\mu = 0.1$, $\phi = 0.8$, $We = 0.6$, and $a = 0.8$.

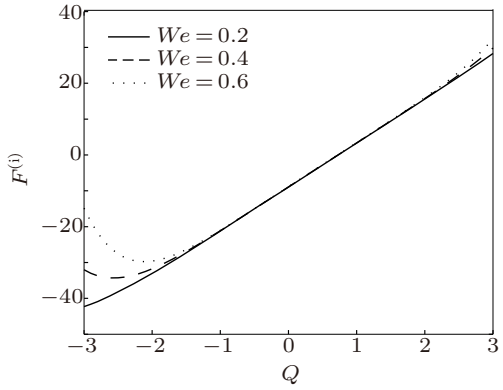


Fig. 11. Frictional force on the outer tube versus flow rate for $\eta = 0.1$, $\mu = 0.2$, $\varepsilon = 0.5$, $\phi = 0.8$, and $a = 0.6$.

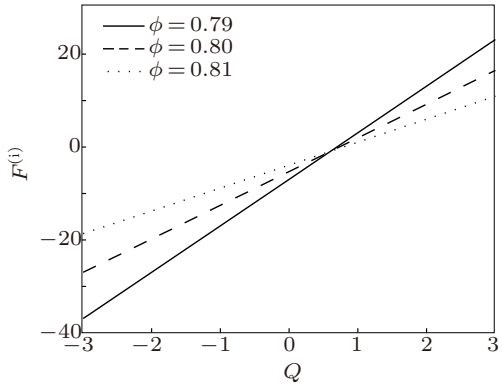


Fig. 12. Frictional force on the outer tube versus flow rate for $\eta = 0.1$, $\mu = 0.1$, $\varepsilon = 0.3$, $We = 0.51$, and $a = 0.7$.

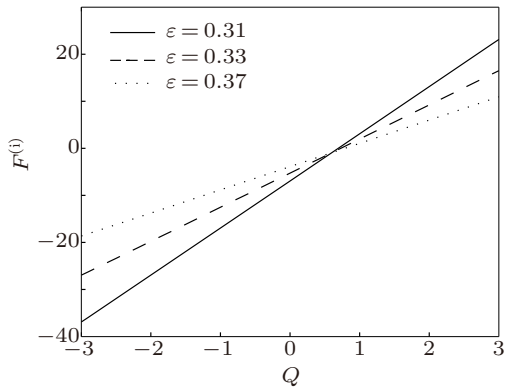


Fig. 13. Frictional force on the outer tube versus flow rate for $\eta = 0.1$, $\mu = 0.1$, $\phi = 0.8$, $We = 0.6$, and $a = 0.8$.

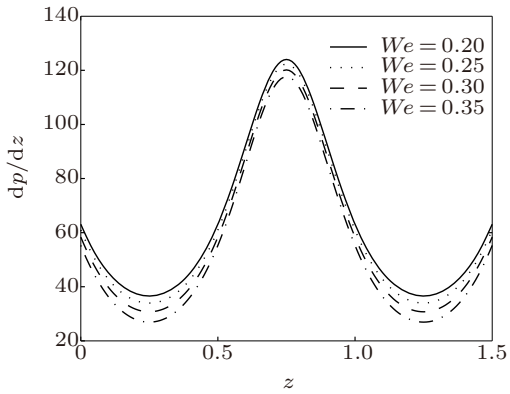


Fig. 14. Pressure gradient versus z for $\eta = 0.01$, $\mu = 0.02$, $\varepsilon = 0.1$, $Q = 5$, $\phi = 0.2$, and $a = 0.02$.

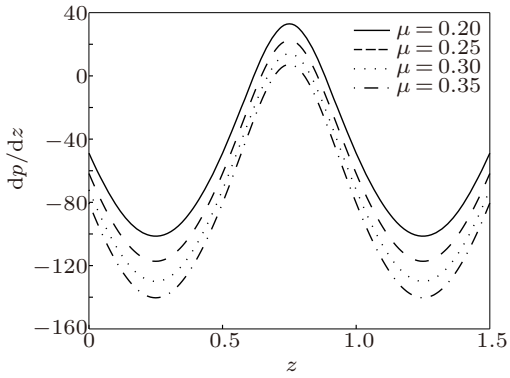


Fig. 15. Pressure gradient versus z for $We = 0.9$, $\eta = 0.02$, $\varepsilon = 0.1, Q = 5$, $\phi = 0.2$, and $a = 0.02$.

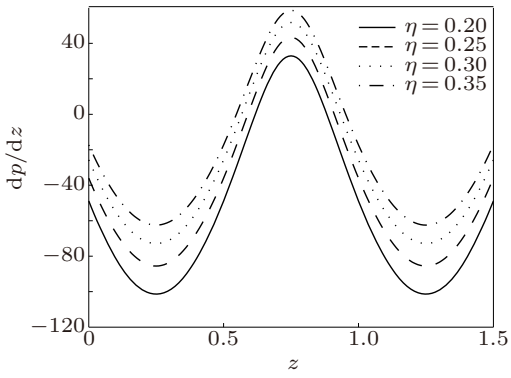


Fig. 16. Pressure gradient versus z for $We = 0.9$, $\mu = 0.02$, $\varepsilon = 0.1$, $Q = 5, \phi = 0.2$, and $a = 0.02$.

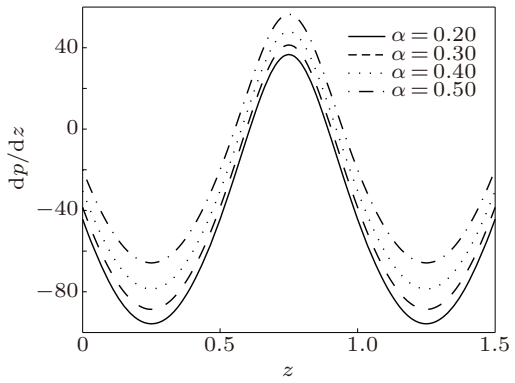


Fig. 17. Pressure gradient versus z for $We = 0.9$, $\eta = 0.02$, $\varepsilon = 0.1, Q = 5$, $\phi = 0.2$, and $\mu = 0.02$.

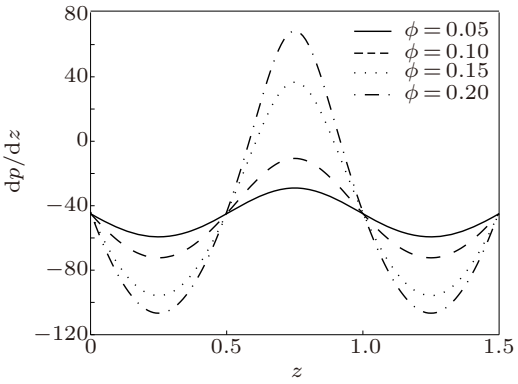


Fig. 18. Pressure gradient versus z for $We = 0.9$, $\eta = 0.02$, $\varepsilon = 0.1, Q = 5$, $a = 0.2$, and $\mu = 0.02$.

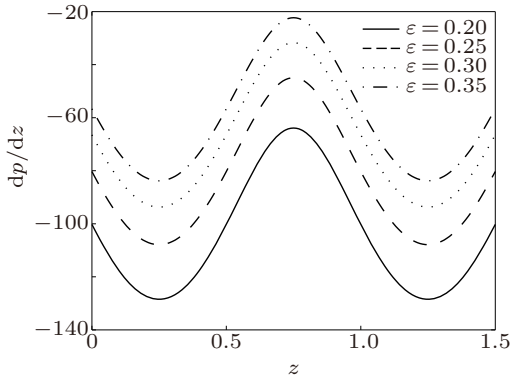


Fig. 19. Pressure gradient versus z for $We = 0.9$, $\eta = 0.02$, $\phi = 0.1, Q = 5$, $a = 0.2$, and $\mu = 0.02$..

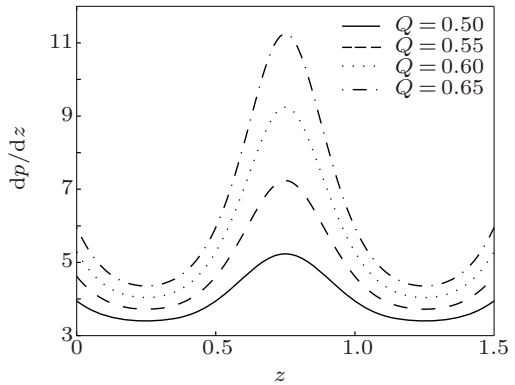


Fig. 20. Pressure gradient versus z for $We = 0.9$, $\eta = 0.02$, $\phi = 0.1$, $Q = 5$, $a = 0.2$, and $\mu = 0.02$.

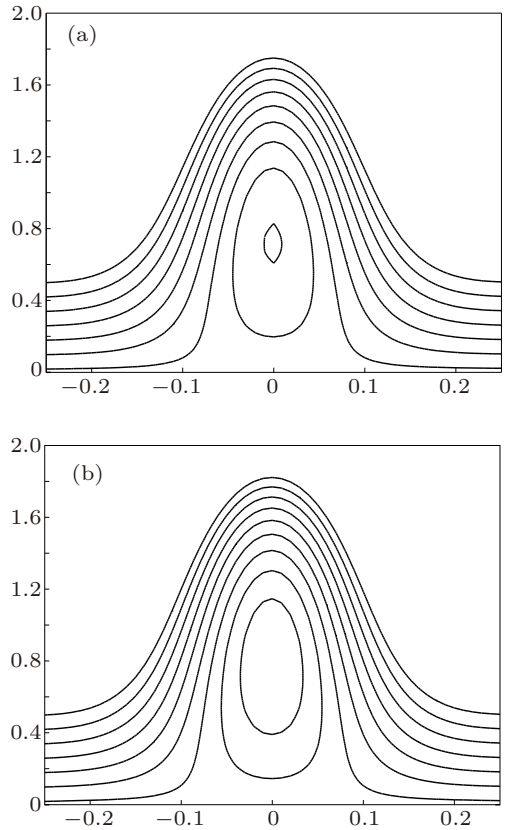


Fig. 21. Streamlines for (a) $Q = 0.1$ and (b) $Q = 0.2$, the other parameters are $We = 0.5$, $\varepsilon = 0.5$, $\phi = 0.1$, $\eta = 0.02$, $\mu = 0.3$, and $a = 0.5$.

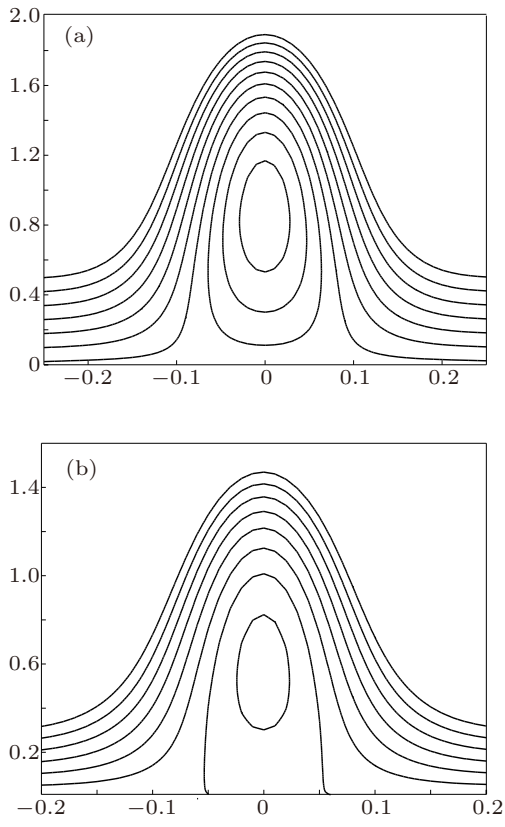


Fig. 22. Streamlines for (a) $\mu = 0.1$ and (b) $\mu = 0.2$, the other parameters are $We = 0.4$, $\varepsilon = 0.5$, $\phi = 0.1$, $Q = 0.5$, $\eta = 0.3$, and $a = 0.5$.

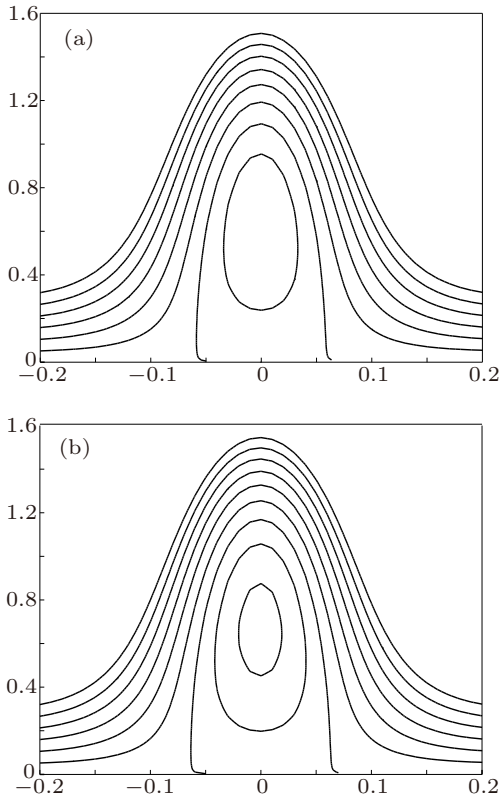


Fig. 23. Streamlines for (a) $\phi = 0.1$ and (b) $\phi = 0.2$, the other parameters are $We = 0.4$, $\varepsilon = 0.5$, $\eta = 0.1$, $Q = 0.5$, $\mu = 0.4$, and $a = 0.5$.

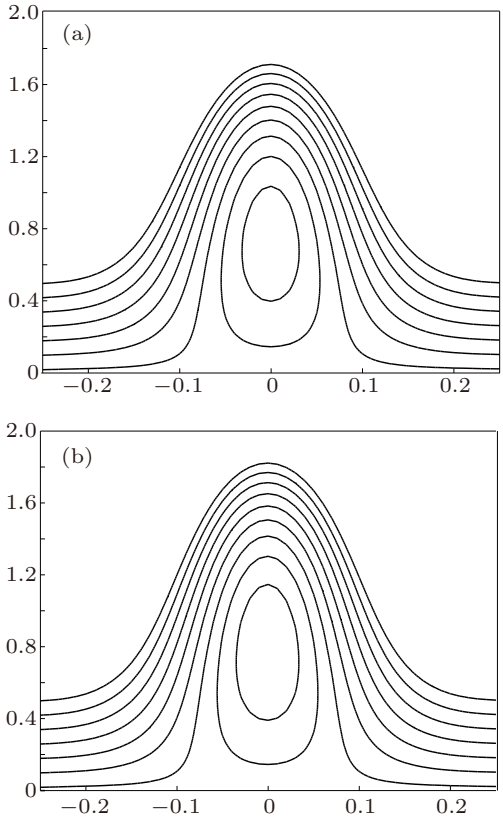


Fig. 24. Streamlines for (a) $We = 0.4$ and (b) $We = 0.6$, the other parameters are $\phi = 0.1$, $\varepsilon = 0.5$, $\eta = 0.2$, $Q = 0.5$, $\mu = 0.3$, and $a = 0.5$.

7. Conclusions

The analytical solutions and the numerical simulation of the peristaltic transport of a Johnson–Segalman fluid in an endoscope are analyzed. Important observations are summed up below.

(i) It is observed that for small perturbation parameter We, we have a good agreement between all the three results, i.e., the HAM, the perturbation, and the numerical solutions, but for large We, the solutions deviate from each other, i.e., the error increases.

(ii) It is also seen that for large values of We, the perturbation solution is not valid, it diverges. But the HAM and the numerical solutions are valid and give convergent solutions.

(iii) It is shown that for large values of a, the numerical, the perturbation, and the HAM solutions are valid.

(iv) The pressure rise and the volume flow rate are inversely proportional to each other.

(v) The pressure rise decreases with the increases of Weisenberg number We, amplitude ratio ϕ, and radius ratio ε.

(vi) The frictional forces and the pressure rise show reverse results.

(vii) The pressure gradient decreases with the increasing We and μ while increases with the increases of η, a, ϕ, ε, and Q. It is also seen that the maximum pressure occurs at the center of the endoscope.

(viii) The size of the trapped bolus increases with the increases of Q, μ, and ϕ but decreases with the increase of We.

(ix) When $We = 0$, we get the results of Newtonian fluid.

References

[1] Nadeem S, Hayat T, Akbar N S and Malik M Y 2009 *Int. J. Heat Mass Transfer.* **52** 4722
[2] Nadeem S and Akbar N S 2009 *Commun. Nonlinear Sci. Numer. Simul.* **14** 3844
[3] Nadeem S, Akbar N S and Malik M Y 2010 *Zeitschrift fur Naturforschung.* **65a** 369
[4] Nadeem S and Akbar N S 2010 *Appl. Math. Comput.* **216** 3606
[5] Latham T W 1966 Fluid Motion in a Peristaltic Pump (Ph. D. Thesis) (Cambridge: Massachusetts Institute of technology)
[6] Srinivas S and Gayathri R 2009 *Appl. Math. Comput.* **215** 185
[7] Ebaid A 2008 *Phys.* A **372** 5321
[8] Srinivasacharya D, Mishra M and Rao A R 2003 *Acta Mech.* **161** 165
[9] Nadeem S and Akbar N S 2009 *Commun. Nonlinear Sci. Numer. Simul.* **14** 4100
[10] Nadeem S, Akbar N S and Vajravelue K 2011 *Int. J. Comput. Math.* **88** 1013
[11] Haroun M H 2007 *Comput. Mater. Sci.* **39** 324
[12] Nadeem S 2007 *Phys. Lett.* A **368** 181
[13] Nadeem S and Ali M 2009 *Commun. Nonlinear Sci. Numer. Simulat.* **14** 2073
[14] Srivastava L M and Srivastava V P 1985 *Ann. Bio. Medical Eng.* **13** 137
[15] Kothandapani M and Srinivas S 2008 *Int. J. Non-linear Mechanics* **43** 915
[16] Srinivas S, Gayathri R and Kothandapani M 2009 *Comput. Phy. Commun.* **180** 2115
[17] Sankar D S and Hemalatha K 2007 *Appl. Math. Comput.* **188** 567
[18] Mekheimer K S and Elmaboud Y E 2008 *Phys.* A **387** 2403
[19] Baris S 2001 *Acta Mech.* **148** 117
[20] Srinivasan U and Rao A R 1995 *J. Biomech.* **28** 45
[21] Hakeem A E, Naby A E, Misery A E M E and Shamy I I E 2004 *Phys.* A **343** 1
[22] Vajravelu K, Sreenadh S and Babu V R 2005 *Int. J. Non-linear Mech.* **40** 83

[23] Johnson M W and Segalman D 1977 *J. Non-Newtonian Fluid Mech.* **2** 255
[24] Kolkka R W, Malkus D S, Hansen M G, IerIy G R and Worthing A R 1988 *J. Non-Newtonian Fluid Mech.* **29** 303
[25] Malkus D S, Nohel J A and Plohr B J 1990 *J. Comput. Phys.* **87** 464
[26] McLeish T C B and Ball R C 1986 *J. Polym. Sci.* (B) **24** 1735
[27] Kraynik A M and Schowalter W R 1981 *J. Rheol.* **25** 95
[28] Rao I J and Rajagopal K R 1999 *Acta Mech.* **132** 209
[29] Ealshahed M and Haroun M H 2005 *Math. Prob. Eng.* **6** 663
[30] Nadeem S and Akbar N S 2009 *Int. Commun. Heat Mass Transfer.* **36** 1050
[31] Hayat A and Ali N 2007 *Appl. Math. Comput.* **188** 1491